Charging Behavior of Single-Stranded DNA Polyelectrolyte Brushes

Supporting Information

Preparation of Electrodes. All experiments used an Ag/AgCl/3M NaCl reference electrode (Bioanalytical Sciences; 0.209 V vs NHE at 25 ^{o}C), and all potentials quoted are relative to this reference. A Pt wire served as the counter electrode. Most of the electrochemical studies used a polycrystalline gold working electrode 3 mm in diameter (Bioanalytical Sciences). Prior to preparation of a DNA monolayer, the working electrode, encased in a polychlorotrifluoroethylene sheath, was mechanically polished with 1 μm diamond slurry followed by 0.05 μm alumina. After polishing, the electrode was rinsed with deionized water and electrochemically etched by potentiodynamic cycling between 0.24 V and 1.54 V in 0.1 M H_2SO_4, 10 mM KCl, using 20 cycles at 100 mV/s scan rate. This protocol provides a reproducible initial surface state [1]. After etching, the electrode was rinsed with deionized (18.2 MΩ cm) water and the roughness factor r (r = true area/geometric area; $r \geq 1$) was measured from the double layer capacitance. Roughness measurements were carried out as in reference 1 except that electrochemical impedance spectroscopy (EIS) rather than AC voltammetry was employed. Values of r ranged from 2.56 to 3.25, with the average being 2.87 ± 0.28. After a final water rinse, the still wetted electrode was immersed in the DNA deposition solution.

Larger Au electrodes, used for XPS measurements (see below), were prepared on glass microscope slides. The slides were first cleaned by immersion for 15 min in 100 ^{o}C, 70/30 solution of concentrated H_2SO_4 and hydrogen peroxide (30 % in water). *Caution: this solution is highly corrosive and oxidizing*. The slides were washed with deionized water and dried under a

nitrogen stream. Cleaned slides were coated with a 20 nm Cr adhesion sublayer and a 1 μm Au overlayer in a thermal evaporator. Immediately prior to immobilization of the DNA, thus prepared working electrodes were potentiodynamically etched as described above for the disk electrodes. After measurement of *r* and a water rinse, the still wetted electrodes were immersed in the DNA deposition solution. For these electrodes *r* ranged from 1.13 to 1.24, with average value of 1.20 ± 0.05, derived for a geometric electrode area of 1.43 cm^2.

Sample Preparation. Single-stranded, Thy_{25}-S-S-$(CH_2)_3$OH oligodeoxyribonucleotides (MWG, HPSF purified) were chemisorbed onto precleaned Au supports from 1 μM solutions in 1 M $MgCl_2$. The disulfide modification was at the 3' strand terminus. Addition of $MgCl_2$ to the deposition solution facilitated achievement of high coverages [2,3]. Strand coverage was controlled by varying the deposition time from a few minutes to several hours. After adsorption of the DNA, the electrodes were immersed for 1 h in 1 mM mercaptopropanol (MCP; Aldrich, 95 % purity) in deionized water. This step displaces nonspecific contacts between the oligonucleotides and the gold and passivates the electrode with a hydrophilic, hydroxyl-terminated self-assembled monolayer (SAM) that helps ensure an end-tethered geometry for the strands [4,5]. An all thymine sequence was used because, of the four bases, thymine exhibits the weakest attraction to gold [6-8] and hence its interaction with gold is easiest to displace with MCP. Because an MCP SAM is only about 0.7 nm thick, its capacitance is relatively high, thus increasing sensitivity of EIS measurements to conditions inside the DNA monolayer (cf. eqn 2 in the main text).

Electrochemical Measurements. A Parstat 2263 potentiostat/galvanostat/frequency response analyzer (Princeton Applied Research), operated by PowerSuite software, was used for all

measurements. Differential capacitance per area, C_d, was measured as a function of Thy_{25} surface coverage and bulk ionic strength using EIS. EIS measurements employed the 3 mm disk electrodes under nominally nonfaradaic conditions and 0 V bias vs Ag/AgCl/3M NaCl, 5 mV ac amplitude, and frequencies from 10 Hz to 100,000 Hz. The electrolyte was gently stirred during measurement. For a given chain coverage on the working electrode, the ionic strength was decreased from a starting concentration of 1 M by serial two-fold dilutions, keeping electrode positions and total solution volume fixed. At each ionic strength, two complete EIS scans were carried out 4 minutes apart; reported C_d values are the average of the two measurements. The working electrode was maintained at the 0 V bias during the 4 min wait times. Use of KCl instead of NaCl produced similar results and data obtained with the two salts were treated equivalently. Ionic strengths lower than 8 mM were not investigated on account of increasing drift in C_d caused by leakage of ions from the reference electrode's internal reservoir.

After completion of EIS scans, the working electrode with the DNA monolayer was rinsed with deionized water and immersed in deoxygenated background electrolyte of 10 mM tris(hydroxymethyl)amino methane (tris base, pH 7.4, adjusted with HCl), followed by immersion in 10 mM tris with 1 μM hexaaminеruthenium(III) chloride (RuHex; Strem Chemicals, 99% purity). Cyclic voltammetry data were obtained under quiescent conditions in both background electrolyte (no RuHex) and in the presence of RuHex at a scan rate of 0.08 V/s. The current-potential (*i*-*V*) curve for the RuHex solution was corrected for charging current by subtraction of the curve for background electrolyte, and the position of the $RuHex^{3+}$ + e- → $RuHex^{2+}$ reduction peak was determined by fitting a quadratic polynomial to the peak maximum. DNA strand coverage was obtained from the position of this peak using an independent calibration against absolute coverages determined with X-ray photoelectron spectroscopy (XPS).

Calculation of the Differential Capacitance C_d from EIS Data. EIS measurements furnish raw data as the frequency (ω) dependent complex impedance $Z(\omega) = \mathrm{Re}(Z) + j\mathrm{Im}(Z)$, where $j = (-1)^{0.5}$. Under nonfaradaic conditions when charge transfer at the working electrode is negligible, the impedance response can be represented as that of an equivalent circuit consisting of two elements in series: (i) a resistor R, representing ohmic conductivity of bulk electrolyte, and (ii) a capacitor AC_d (A: area of capacitor; C_d: differential capacitance per area), representing charging of the interface between bulk electrolyte and the working electrode (WE). For such a circuit, $Z = R - j/(\omega AC_d)$, with a phase angle given by $\phi = \arctan(\mathrm{Im}(Z)/\mathrm{Re}(Z)) = \arctan(-1/(\omega AC_d R))$ [9]. The phase will therefore vary from close to 0 ^{o} at high frequencies, when the sample is behaving nearly as a pure (real) resistance with only a small (imaginary) capacitive impedance, to - 90 ^{o} at low frequencies when the WE/electrolyte interface has time to charge fully and the out-of-phase, capacitive impedance dominates. At intermediate frequencies both resistive and capacitive impedances contribute to the measured response. Fig. S1 shows an example of EIS data obtained at high and low ionic strengths.

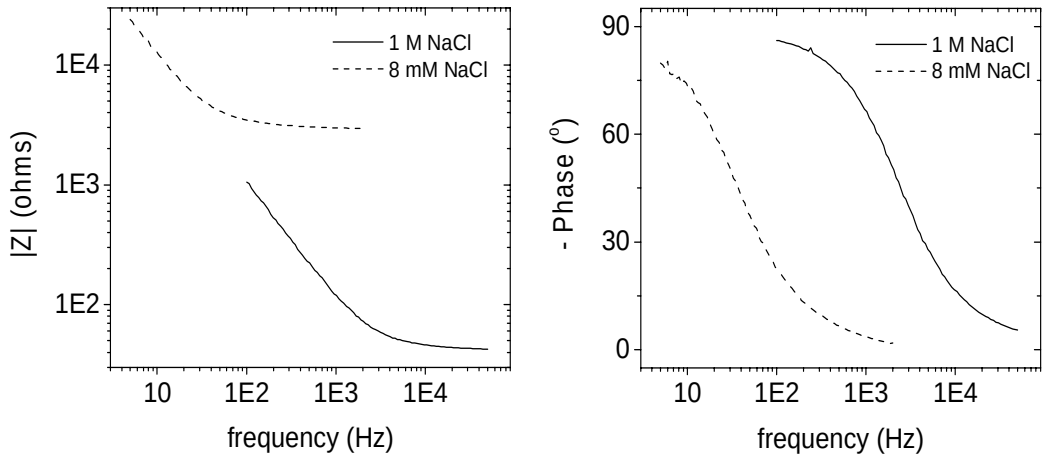

Figure S1. Example of EIS data at high (1M NaCl) and low (8mM NaCl) ionic strengths. Conditions: pH 7.0 solution of indicated ionic strength, no buffering agent, 5 mV rms ac amplitude, 0 V dc vs Ag/AgCl/3M NaCl. Strand coverage: 7.8×10^{12} cm^{-2}.

Experimental calculation of C_d values reported in the main text used the symmetrically located region between $-70\ ^{o} < \phi < -20\ ^{o}$. Selection of this region was motivated by a desire to avoid very low frequencies at which slow electron transfer processes can become noticeable [10-12], and highest frequencies at which the electrode interface contributes negligibly to the overall impedance. For a parallel plate capacitor in an RC circuit, selection of a fixed range of phase angles corresponds to application of a fixed range of electric fields across the capacitor. For comparison, C_d values were also calculated using all data points, as well as those falling in the smaller range $-80\ ^{o} < \phi < -40\ ^{o}$. All three choices for regions of analysis closely reproduced the experimental trends presented in Figs. 3 and 5 of the main text. Quantitatively, the flattening of the C_d vs ionic strength curves at greater strand coverages was slightly less when all data points were included. When all the points were included, the increase in C_d as ionic strength was raised from 8 mM to 1 M for the highest coverage sample (2.1×10^{13} cm^{-2}) was 0.23 times that

observed without DNA (pure MCP sample), compared to 0.20 when only points in the range -70 $^{o} < \phi <$ - 20 ^{o} were used.

To calculate C_d, the experimental Z data were interpreted in the context of a series R-Q model, where Q represents a constant phase element, or CPE [13], that was used in place of an ideal capacitor representation of the electrode surface. A CPE accounts for inhomogeneity of real interfaces (e.g. due to roughness or chemical variability) that leads to heterogeneity in the double layer and variations in current density along the electrode surface [10,14,15]. The impedance of a CPE element is $1/((j\omega)^n G)$, from which the equivalent capacitance per area C_d is calculated using [13]

$$C_d = (R^{1-n} G)^{1/n}/A \qquad \text{(S1)}$$

where the true electrode area $A = rA_G$ (r: roughness factor, A_G: geometric area of the electrode). Physically, C_d can be defined in terms of the RC relaxation time for charging of the double layer [13]. For n = 1, the CPE reduces to the behavior of an ideal capacitor. R, G and n were derived by fitting of EIS data, and r was determined as described above. The experimental values of n ranged from 0.953 to 0.979. Typical uncertainties (= 100 × variance/parameter value) in the fitted values of R, G, and n were 0.6 %, 3 %, and 0.4 %, respectively.

Calculations were also performed using a model in which a second resistor, R_{SAM}, was placed in parallel with the CPE to allow for possibility of charge transfer across the MCP layer. Analysis of the data with this more complicated model yielded R_{SAM} values ranging from ~ 1×10^{14} Ω to ~ 1×10^{20} Ω, accompanied by an occasional change in values of R, G, or n at the fourth significant digit compared to those derived with the simpler series R-Q model. These differences

were immaterial to interpretation of the EIS data; therefore, the values derived from the simpler *R-Q* model were used.

XPS Measurements. XPS was used to provide absolute calibration for the determination of strand coverage. Measurements were performed on a Kratos Axis 165 instrument with a hemispherical analyzer using Mg Kα source. The parameters set for all the measurements were: 225 W x-ray power, 120 μm spatial resolution with corresponding aperture and iris settings, 52.5^{o} angle between incident X-ray photons and collected photoelectrons, 80 eV pass energy, and 90^{o} (normal to sample) takeoff angle. A wide pass energy was used to improve signal intensity at the expense of energy resolution. Energy shifts were observed without charge neutralization, attributed to electrical insulation by the underlying glass slide support on which samples were prepared; therefore, measurements were performed with the charge neutralizer on. Binding energies, where reported, are relative to the Au $4f_{7/2}$ line being set at 84.0 eV. Samples were scanned for Au 4f, P 2p, S 2p, C 1s, N 1s, and O 1s lines.

Line intensities were calculated from peak areas after subtraction of the inelastic background, with the background modeled by Shirley functions. DNA coverages were calculated from thus obtained P 2p intensities following the procedure of Petrovykh *et al* [16]. These authors have recently published a thorough XPS analysis of thiolate-anchored single-stranded Thy_{25} monolayers on gold. The main difference with the samples investigated in this study is the additional use of MCP passivation in the present case.

Calculation of DNA coverage required the following two equations [17]:

Intensity I_i emitted from element *i* distributed uniformly throughout a film of thickness *t*:

$$I_i = R_i \rho_i X_i \Lambda_i^Q (1 - \exp(-t/\Lambda_i^P \sin\theta)) \quad \text{(S2)}$$

Intensity I_i emitted from element i distributed uniformly in a semi-infinite body that is covered by overlayers A and B of thickness t^A and t^B, respectively:

$$I_i = R_i \rho_i X_i \Lambda_i^Q \exp(-t^A/\Lambda_i^{PA} \sin\theta) \exp(-t^B/\Lambda_i^{PB} \sin\theta) \quad \text{(S3)}$$

Eqn S2 is applicable to photoelectrons emitted from atoms in the DNA monolayer, which is the topmost film. Eqn S3 is applicable to photoelectrons emitted from atoms in the gold support, which is covered by two overlayers; e.g. layer A is the MCP film and layer B the DNA layer. The quantities in eqns S2 and S3 are defined as follows:

R_i = instrumental response function accounting for intensity of the X-ray source, solid angle from which photoelectrons emitted by element i are collected, and efficiency of the instrument's analyzer in detecting the photoelectrons. R_i depends on the kinetic energy of the photoelectrons.

ρ_i = number density (atoms/volume) of the element being measured

X_i = differential photoionization cross-section for element i

Λ_i^Q = effective attenuation length for quantitative analysis of semi-infinite samples for photoelectrons emitted by element i, as defined in reference [18]. Λ_i^Q was calculated at the kinetic energy of the photoelectrons using the NIST Standard Reference Database 82 (SRD-82) software [19] and material properties taken from literature (Table S1).

Λ_i^P = average practical attenuation length for analysis of film samples containing element *i*, as defined in reference [18]. Λ_i^P was calculated at the kinetic energy of the photoelectrons of interest using the NIST SRD-82 software [19] and material properties taken from literature (Table S1).

θ = take-off angle of measured photoelectrons (analyzer to sample horizontal)

Using eqn S2 for P 2p emission from the DNA monolayer and eqn S3 for Au 4f emission from the gold support leads to the following expression for the ratio of the respective intensities

$$I_P / I_{Au} = \frac{R_P \rho_P X_P \Lambda_P^Q (1 - \exp(-t^{DNA} / \Lambda_P^{P,DNA} \sin\theta))}{R_{Au} \rho_{Au} X_{Au} \Lambda_{Au}^Q \exp(-t^{MCP} / \Lambda_{Au}^{P,MCP} \sin\theta) \exp(-t^{DNA} / \Lambda_{Au}^{P,DNA} \sin\theta)} \quad \text{(S4)}$$

This expression can be simplified since $\theta = 90^o$ and since the *R* values at the P 2p (binding energy 134.1 eV, kinetic energy 1120 eV) and Au 4f (binding energy 84.0 eV, kinetic energy 1170 eV) lines are nearly identical, i.e. R_P very nearly equals R_{Au} and the response functions cancel. The unknown thickness of the DNA film, t^{DNA}, can be expressed in terms of the surface amount (atoms/area) of DNA P atoms, Γ_P, using $t^{DNA} = \Gamma_P / \rho_P$. These rearrangements lead to

$$\frac{1 - \exp(-\Gamma_P / \rho_P \Lambda_P^{P,DNA})}{\exp(-\Gamma_P / \rho_P \Lambda_{Au}^{P,DNA})} = \frac{I_P \rho_{Au} X_{Au} \Lambda_{Au}^Q}{I_{Au} \rho_P X_P \Lambda_P^Q \exp(t^{MCP} / \Lambda_{Au}^{P,MCP})} \quad \text{(S5)}$$

Table S1 lists the various parameters needed in eqn S5 for calculation of Γ_P, the unknown of interest. From Γ_P, the strand coverage σ_{DNA} is obtained using

$$\sigma_{DNA} = \Gamma_P / 25r \quad \text{(S6)}$$

where division by the roughness factor r ($r \approx 1.2$) provides an approximate correction for surface roughness and there are 25 P atoms per one Thy_{25} strand.

Table S1. Parameters for calculation of Γ_P

ρ_P (cm^{-3}) [A]	ρ_{Au} (cm^{-3}) [B]	X_P (cm^2) [C]	X_{Au} (cm^2) [C]	t^{MCP} (cm) [D]	$\Lambda_P^{P,DNA}$ (cm) [E]	$\Lambda_{Au}^{P,DNA}$ (cm) [E]	Λ_P^{Q} (cm) [E]	Λ_{Au}^{Q} (cm) [E]	$\Lambda_{Au}^{P,MCP}$ (cm) [F]
1.75e21	5.90e22	2.06e-21	2.91e-20	6.7e-8	3.2e-7	3.3e-7	3.3e-7	1.5e-7	2.8e-7

[A] Calculated using mass density for Thy_{25} monolayers of d = 0.89 g/cm^3, as determined by Petrovykh and coworkers under vacuum conditions with XPS [16], and strand molar mass m of 7690 g/mol. $\rho_P = (d/m)*25N_A$ where N_A is Avogadro's number and there are 25 P atoms per strand.
[B] Obtained using bulk density of gold of 19.3 g/cm^3.
[C] Taken from Scofield tables for Mg Kα x-rays [20], using asymmetry parameters 1.18 for P 2p and 1.01 for Au 4f [19].
[D] Estimated from mass density of MCP, d = 1.07 g/cm^3, molar mass of MCP, m = 92 g/mol, and surface coverage of alkanethiol monolayers on gold σ = 4.7e14 molecules/cm^2 [21]. $t^{MCP} = \sigma m/(d\ N_A)$.
[E] Calculated using NIST SRD 82, Version 1.0 [19], for Mg Kα x-rays. Following Petrovykh *et al* [16], the bandgap energy of Thy_{25} molecules was taken to be 4.8 eV and the mass density 0.89 g/cm^3. Average practical attenuation lengths (Λ_i^P) were calculated for 5 nm films. Detailed discussion of these parameters and settings is provided in reference [16]. The number of valence electrons per strand was determined to be 2781 based on the atomic composition of Thy_{25}.
[F] Calculated from Λ = 3e-9 $KE^{0.64}$ cm where KE is the photoelectron kinetic energy, as reported for alkanethiol monolayers on gold by Lamont and Wilkes [22].

Since the values of $\Lambda_P^{P,DNA}$ and $\Lambda_{Au}^{P,DNA}$ are nearly identical (Table S1), eqn S5 can be simplified further by setting both of these parameters to $\Lambda^{P,DNA}$ = 3.25E-7 cm,

$$\exp(\Gamma_P / \rho_P \Lambda^{P,DNA}) - 1 = \frac{I_P \rho_{Au} X_{Au} \Lambda_{Au}^{Q}}{I_{Au} \rho_P X_P \Lambda_P^{Q} \exp(t^{MCP} / \Lambda_{Au}^{P,MCP})}$$

what rearranges to

$$\Gamma_P = \rho_P \Lambda^{P,DNA} \ln\left[1 + \frac{I_P \rho_{Au} X_{Au} \Lambda_{Au}^{Q}}{I_{Au} \rho_P X_P \Lambda_P^{Q} \exp(t^{MCP} / \Lambda_{Au}^{P,MCP})}\right] \quad \text{(S7)}$$

Thy_{25} strand coverages σ_{DNA} were calculated from eqns S7 and S6. Except for the inclusion of the exponential factor in the denominator of the ln term in eqn S7, which corrects for attenuation by the MCP monolayer, this equation is equivalent to eqn 9 in reference [16].

Estimation of the Ratio r_D/H inside a DNA Brush.

The value of the Debye screening r_D is estimated from the formula $r_D = (\varepsilon\varepsilon_0 RT / 2N_A^2 e^2 c_{ES})^{1/2}$ where c_{ES} is molar concentration of monovalent charges capable of reorganizing their distribution, and hence contributing to electrostatic screening, in response to the ac modulation used to measure C_d. ε and ε_0 are the solution dielectric constant and electric permittivity of vacuum, respectively. Since polyelectrolyte brush systems such as the DNA films are expected to be close to electroneutral [23,24], c_{ES} must be at least as large as c_{CI}, the concentration of Na^+ counterions needed to compensate the negative DNA charge. When salt is present, as in the experiments, it will further increase the ionic strength in the brush leading to $c_{ES} > c_{CI}$. Thus $c_{ES} > c_{CI}$ where $c_{CI} \approx Q\sigma_{DNA}/N_A H$, with Q the number of mobile counterions per strand. Only those counterions that are mobile (i.e. uncondensed on the DNA backbone[25,26]) are expected to contribute to electrostatic screening. For ssDNA, Q is about 60 % of the total phosphate charge [26]; thus $Q \approx 15$ for a 25mer strand.

The above considerations yield $r_D/H < (\varepsilon\varepsilon_0 RT / 2N_A e^2 Q\sigma_{DNA} H)^{1/2}$. It is evident that, for the present experiments, an upper limit on this ratio will be obtained by using the lowest chain

coverage studied, $\sigma_{DNA} = 2.4 \times 10^{12}$ cm^{-2}, and the smallest brush thickness H_{MIN} expected. A good estimate for H_{MIN} is 4.8 nm, as found by neutron reflectivity measurements for a similar brush of 25mer oligonucleotides at a coverage of 3×10^{12} cm^{-2} in 1 M NaCl[5,27]. This value for H is expected to be a minimum because, at the generally lower ionic strengths and greater chain coverages of the present study, the brushes are expected to swell leading to larger H. Inserting the above values yields $r_D < 0.9$ nm and $r_D/H < 0.9/4.8 = 0.19$. That r_D is predicted to be significantly less than H supports the model outlined in Fig. 4. of the main text, with a brush body region that is largely free of the electrostatic influence of the surface.

Derivation of Equation 3 for C_{DL}. From the Poisson equation, applied at a planar solid-liquid interface

$$\frac{d^2V}{dx^2} = \frac{-\rho(x)}{\varepsilon\varepsilon_0} \tag{S8}$$

where $V(x)$ is the potential as a function of the distance x from the solid-liquid interface, ρ is charge per unit volume, ε is the dielectric constant of the medium (assumed constant), and ε_0 is the permittivity of vacuum. ρ equals the sum of the DNA charge $\rho_{DNA} = -eN_A c_{DNA}$ (N_A: Avogadro's number, c_{DNA}: molar concentration of DNA charge) and the concentrations $\rho_+ = eN_A c_+$ of positive (i.e. Na^+) and $\rho_- = -eN_A c_-$ of negative (i.e. Cl^-) monovalent ions. Contributions due to autoionization of water are neglected. The DNA charge is assumed immobile and of constant concentration in the region $0 < x < H$ occupied by the brush, and zero outside that region. Computer simulations show that, for a highly-charged polyelectrolyte brush, the segment profile indeed tends to a step-like distribution at higher chain coverages and lower ionic

strengths[23]. Notably, the assumption of a uniform, step-like DNA segment distribution neglects influence of the potential $V(x)$ on the DNA organization. The charge densities of the small ions, ρ_+ and ρ_-, are functions of the local potential according to the usual Boltzmann weighing,

$$\rho_{\pm}(x) = \pm eN_A c_{\pm}(x) = \pm eN_A c_{\pm}^{\infty} e^{\mp V(x)e/kT} \tag{S9}$$

where the superscript ∞ denotes concentrations in the body of the brush, beyond the proximal region (see Fig. 4 in the main text). Here, the body of the brush acts as the "bulk" electrolyte with which the nonuniform ion distribution in the proximal region is in equilibrium. Equation S9 rests on the stipulation that r_D/H inside the DNA layer is significantly less than 1, as discussed above. Combining S8 and S9

$$\frac{\varepsilon\varepsilon_0}{eN_A}\frac{d^2V}{dx^2} = c_{DNA} + c_-^{\infty} e^{V(x)e/kT} - c_+^{\infty} e^{-V(x)e/kT} \tag{S10}$$

Integrating once with the boundary condition $V_\infty = (\mathrm{d}V/\mathrm{d}x)_\infty = 0$ yields (where, again, ∞ refers to the brush body)

$$\left(\frac{\varepsilon\varepsilon_0}{2eN_A}\right)^{1/2}\frac{dV}{dx} = \pm\left(c_{DNA}V + \frac{kTc_-^{\infty}}{e}(e^{V(x)e/kT} - 1) + \frac{kTc_+^{\infty}}{e}(e^{-V(x)e/kT} - 1)\right)^{1/2} \tag{S11}$$

where the upper (+) sign applies when $V_0 < 0$ and the lower (-) sign when $V_0 > 0$. The electric field - dV/dx at $x = 0$ (at the MCP/brush interface) is related to the charge density q on the working electrode by Gauss' Law,

$$\frac{q}{\varepsilon\varepsilon_0} = -\left.\frac{dV}{dx}\right|_{x=0} = \mp\left(\frac{2eN_A}{\varepsilon\varepsilon_0}\right)^{1/2}\left(c_{DNA}V_0 + \frac{kTc_-^\infty}{e}(e^{V_0e/kT} - 1) + \frac{kTc_+^\infty}{e}(e^{-V_0e/kT} - 1)\right)^{1/2} \quad \text{(S12)}$$

In equation S12 q is entirely attributed to charge in the working electrode as the MCP layer is not charged. The differential double layer capacitance C_{DL} is calculated from $C_{DL} = dq/dV_0$. Using equation S12,

$$C_{DL} = \mp\left(\frac{eN_A\varepsilon\varepsilon_0}{2}\right)^{1/2}\frac{c_{DNA} + c_-^\infty e^{V_0e/kT} - c_+^\infty e^{-V_0e/kT}}{\left(c_{DNA}V_0 + \frac{kTc_-^\infty}{e}(e^{V_0e/kT} - 1) + \frac{kTc_+^\infty}{e}(e^{-V_0e/kT} - 1)\right)^{1/2}} \quad \text{(S13)}$$

Because the brush body is nearly electroneutral, $c_{DNA} \approx c^\infty{}_+ - c^\infty{}_-$. Dropping the ∞ superscript ($c^\infty{}_+ \rightarrow c_+$ and $c^\infty{}_- \rightarrow c_-$) then yields the final form as in equation 3 of the text,

$$C_{DL} = \mp\left(\frac{eN_A\varepsilon\varepsilon_0}{2}\right)^{1/2}\frac{c_+(1 - e^{-V_0e/kT}) + c_-(e^{V_0e/kT} - 1)}{\left((c_+ - c_-)V_0 + \frac{kTc_-}{e}(e^{V_0e/kT} - 1) + \frac{kTc_+}{e}(e^{-V_0e/kT} - 1)\right)^{1/2}} \quad \text{(S14)}$$

Full Citations from the Main Text Involving More than 10 Authors.

Citation #4:

Matsuzaki, H.; Loi, H.; Dong, S.; Tsai, Y. Y.; Fang, J.; Law, J.; Di, X. J.; Liu, W. M.; Yang, G.; Liu, G. Y.; Huang, J.; Kennedy, G. C.; Ryder, T. B.; Marcus, G. A.; Walsh, P. S.; Shriver, M. D.; Puck, J. M.; Jones, K. W.; Mei R. *Genome Res.* **2004**, *14*: 414-425.

References for Supporting Information

(1) Oesch, U.; Janata, J. *Electrochim. Acta* **1983**, *28*, 1237-1246.
(2) Petrovykh, D. Y.; Kimura-Suda, H.; Whitman, L. J.; Tarlov, M. J. *J. Am. Chem. Soc.* **2003**, *125*, 5219-5226.
(3) Kelley, S. O.; Barton, J. K.; Jackson, N. M.; McPherson, L. D.; Potter, A. B.; Spain, E. M.; Allen, M. J.; Hill, M. G. *Langmuir* **1998**, *14*, 6781-6784.
(4) Herne, T. M.; Tarlov, M. J. *J. Am. Chem. Soc.* **1997**, *119*, 8916-8920.
(5) Levicky, R.; Herne, T. M.; Tarlov, M. J.; Satija, S. K. *J. Am. Chem. Soc.* **1998**, *120*, 9787-9792.
(6) Kimura-Suda, H.; Petrovykh, D. Y.; Tarlov, M. J.; Whitman, L. J. *J. Am. Chem. Soc.* **2003**, *125*, 9014-9015.
(7) Storhoff, J. J.; Elghanian, R.; Mirkin, C. A.; Letsinger, R. L. *Langmuir* **2002**, *18*, 6666-6670.
(8) Wolf, L. K.; Gao, Y.; Georgiadis, R. M. *Langmuir* **2004**, *20*, 3357-3361.
(9) Bard, A. J.; Faulkner, L. R. *Electrochemical Methods: Fundamentals and Applications*; 2nd ed.; Wiley & Sons, Inc.: New York, 2000.
(10) Protsailo, L. V.; Fawcett, W. R. *Electrochim. Acta* **2000**, *45*, 3497-3505.
(11) Sur, U. K.; Lakshminarayanan, V. *J. Coll. Interface Sci.* **2002**, *254*, 410-413.
(12) Hinnen, C.; Nguyen Van Huong, C.; Rousseau, A.; Dalbera, J. P. *J. Electroanal. Chem.* **1979**, *95*, 131-146.
(13) Brug, G. J.; van den Eeden, A. L. G.; Sluyters-Rehbach, M.; Sluyters, J. H. *J. Electroanal. Chem.* **1984**, *176*, 275-295.
(14) Kerner, Z.; Pajkossy, T. *Electrochim. Acta* **2000**, *46*, 207-211.
(15) Scheider, W. *J. Phys. Chem.* **1975**, *79*, 127-136.
(16) Petrovykh, D. Y.; Kimura-Suda, H.; Tarlov, M. J.; Whitman, L. J. *Langmuir* **2004**, *20*, 429-440.
(17) Fadley, C. S. *Prog. Surf. Sci.* **1984**, *16*, 275-388.
(18) Jablonski, A.; Powell, C. J. *Surf. Sci. Rep.* **2002**, *47*, 33-91.
(19) Powell, C. J.; Jablonski, A. *NIST Electron Effective-Attenuation-Length Database - Version 1.0*; National Institute of Standards and Technology: Gaithersburg, MD, 2001.
(20) Scofield, J. H. *J. Electron. Spectrosc.* **1976**, *8*, 129-137.
(21) Strong, L.; Whitesides, G. M. *Langmuir* **1988**, *4*, 546-558.
(22) Lamont, C. L. A.; Wilkes, J. *Langmuir* **1999**, *15*, 2037-2042.
(23) Kumar, N. A.; Seidel, C. *Macromolecules* **2005**, *38*, 9341-9350.
(24) Israels, R.; Leermakers, F. A. M.; Fleer, G. J.; Zhulina, E. B. *Macromolecules* **1994**, *27*, 3249-3261.
(25) Manning, G. S. *Accts. Chem. Res.* **1979**, *12*, 443-449.
(26) Record, M. T.; Anderson, C. F.; Lohman, T. M. *Quart. Rev. Biophys.* **1978**, *11*, 103-178.
(27) For an ssDNA monolayer of uniform internal composition, of thickness H, the z-rms thickness defined in ref 5 is equal to $H/12^{1/2}$.